Ocean Systems Engineering, *Vol. 16, No. 2 (2026) 207-218*
https://doi.org/10.12989/ose.2026.16.2.207

Techno-Press

Transient response of a floating bridge due to sudden failure of a mooring line under seabed earthquakes

Ikjae Lee, MooHyun Kim*

Department of Ocean Engineering, Texas A&M University, College Station, TX 77843, USA

(Received April 22, 2026, Revised June 7, 2026, Accepted June 10, 2026)

Abstract. In this study, we investigate transient responses of a floating bridge due to the sudden failure of a mooring line under seismic excitations. A straight 4,600-m-long discrete-pontoon floating bridge designed for Bjørnafjord on West Coast of Norway and moored in a water depth of 300 m is employed. A mid-fidelity time-domain-numerical-simulation coupled dynamics model was built by using a commercial software OrcaFlex. Pre-generated site-specific multi-directional ground motion time-series were imposed at all anchors of mooring lines assuming simultaneous movement. Subsequent dynamic responses of pontoons, structural responses of girders, and fairlead mooring tensions are examined for three different scenarios (i) intact, (ii) 1-line pre-failure (iii) 1-line sudden-failure cases. From the numerical results and pertinent analyses, it has been observed that transient responses of the pontoons and girders in the sudden-failure case can be significant and the resulting dynamic quantities become larger than those of intact and pre-failure cases. In the case of a pre-failed line, the transient effects are absent, and it will lead to underestimation in girder's dynamic bending moments and maximum mooring tensions. The effects of the transient motions become appreciable especially for girder's transverse bending moments and adjacent mooring dynamic tensions. The maximum mooring tension is observed in the sudden-failure scenario at the neighboring lines of the failed line as a result of the transient effects.

Keywords: discrete pontoon; girder bending moment; mooring tension; seabed earthquakes; straight floating bridge; transient response

1. Introduction

Floating bridges offer a promising solution for spanning long distances in deep waters, particularly in cases where traditional bottom-fixed bridges prove less economically viable [1]. There are three main designs for floating bridges: the discrete pontoon type, continuous pontoon type, and floating tower and cable-supported type. The design can also be classified into curved and straight bridges. The present study focuses on a straight discrete-pontoon floating bridge designed for Bjørnafjord on West Coast of Norway [2, 3, 4].

Floating bridges may be subject to complex environmental loads. Several studies have been conducted experimentally and numerically by several researchers [5-9]. Further, Jin et al. [10] investigated the feasibility of a tuned mass damper for a curved floating bridge subjected to wind and wave excitations. In particular, Jang et al. [1] studied the effect of sudden failure of tethers and

*Corresponding author, Professor, E-mail: m-kim3@tamu.edu

http://www.techno-press.org/ose/5

ISSN: 2093-6702 (Print), 2093-677X (Online)

cables for a cable-stayed bridge under irregular waves. An analogous study has been conducted by the present authors [11] where dynamic responses of a straight floating bridge was investigated for a pre-failed mooring condition under seismic excitations without transient effects. However, during seismic activity, the holding capacity of soil for anchors becomes weaker due to liquefaction, and accordingly sudden-failure of mooring lines may occur during a short time window of earthquakes. In this regard, we extend our previous study to a scenario of sudden-failure during submarine earthquakes to investigate the effects of transient motions. In order to better explore the transient effects, we checked dynamic responses of pontoons, girders, and mooring lines for three different scenarios: (i) intact (ii) 1-line pre-failure before simulations (iii) 1-line sudden failure in the middle of the simulation. In case of (iii), the transient-motion-induced loading on the bridge girder can be significantly amplified, which is the main objective of the present study.

Multi-directional (3-axes) ground motion time-series are generated and imposed on all anchors of the mooring lines at the target floating bridge model. The pertinent coupled dynamics were carried out through time-domain simulations using a commercial program OrcaFlex. The differences in dynamics time series between the intact and failed conditions may be utilized in developing AI (artificial intelligence)-based automatic mooring-line failure detection [12, 13]. It should be noted that the present study does not consider the effect of fluid disturbance through fluid compressibility, i.e., the seaquake load, generated by ground motion. The compressibility of fluid is known to play a crucial role in the seaquake load as discussed by Lee and Kim [14].

The paper consists of 4 sections. In Section 2, a general description of target floating bridge is described. In Section 3, numerical simulation and results are presented with analyses for the selected load cases. Finally, the paper is concluded with several remarks in Section 4.

2. A straight floating bridge

Main particulars of an idealized straight and side-anchored floating pontoon bridge and mooring lines are detailed in [3], and their short descriptions are summarized in this section. The idealized floating pontoon bridge model is sketched in Figs. 1(a) and 1(b). The total length of the bridge spans 4,600 meters, with a separation distance of 125 meters between neighboring pontoons. The columns, standing at 14.5 meters in height, are rigidly connected to both the upper surface of the pontoons and the lower surface of girders. Mooring lines, as depicted in Figs. 1(a), are fastened to four specific pontoons spaced 1,000 meters apart, each comprising eight strands forming a single cluster, and anchored in a water depth of 300 m. Specifications of mooring lines are provided in Table 1. Fig. 2 illustrates the geometry of a single pontoon model which is used for radiation and diffraction hydrodynamic analysis [15]; the waterplane area shape comprises segments of five circles. In the present idealized model, the center of flotation aligns with the center of gravity, and the spacing between neighboring pontoons ensures that multi-body hydrodynamic interactions between adjacent pontoons are negligible. A mid-fidelity-level numerical model of the floating bridge was built in a commercial software OrcaFlex [16]. In OrcaFlex, coupled time-domain dynamic simulations are performed based on Cummins-type equation of motions [17]. The left end of the bridge is clamped while the right end is hinged in y and z direction but free to move in x direction. More details on the numerical modeling is described in [3].

The transient responses of the floating bridge occur at its natural frequencies. Therefore, its

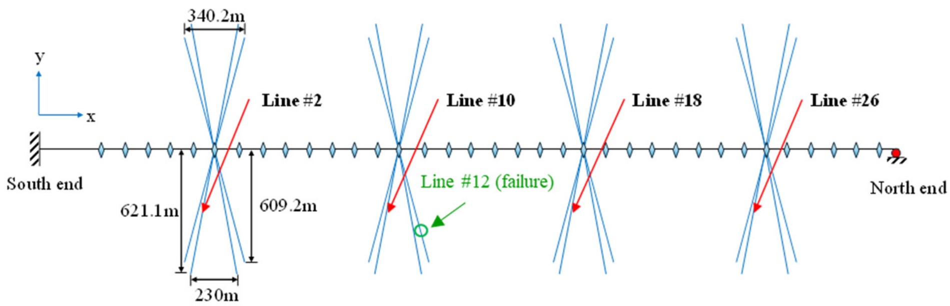

(a) Plan view

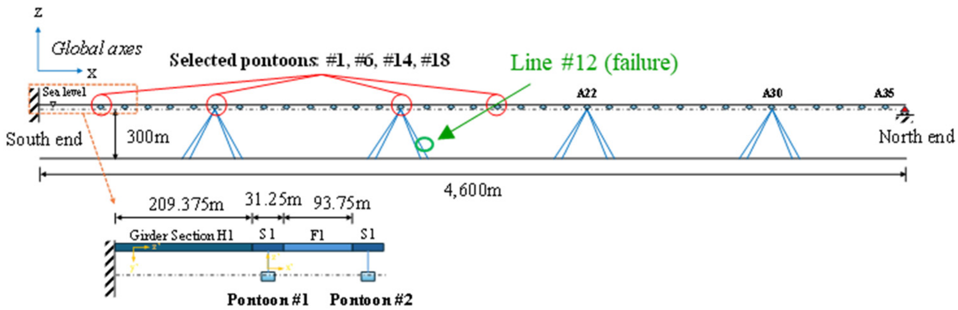

(b) Side view

Figure 1. Idealized straight floating bridge: (a) plan and (b) side view

Table 1. Mooring line specifications

Segment	Nominal Diameter (mm)	Length (m)	Mass (te/m)	Axial stiffness (kN)
Top Chain	147	50	0.4735	1.95e6
Wire	124	600	0.0632	950e3
Bottom Chain	147	50	0.4735	1.95e6

important natural frequencies are summarized in Table 2. The present results are also compared with other researchers' results. In particular, the y-directional transverse dynamics at its lowest natural frequency can play an important role.

3. Numerical results and analyses/discussions

3.1 Load cases

Seismic excitations are based on three different scenarios: intact (I); 1-line pre-failure (F); 1-line sudden failure (T) as tabulated in Table 3. In all three scenarios, mooring line # 12 is assumed to fail, and all the simulations last for 12 minutes. Detailed numerical setting is described in previous studies by the present authors [3, 11]. The multi-directional ground acceleration time histories are available in USGS NSMP (National Strong-Motion Project) Earthquake Date Sets.

Table 2. Comparison of natural periods

Mode	Dominant axis	Natural period [2]	Natural period [4]	Natural period (Reproduced)
1st	y-axis (transverse)	34.1s	34.4s	32.2s
2nd	y-axis	31.2s	30.9s	31.5s
3rd	y-axis	30.3s	29.0s	28.5s
4th	y-axis	20.1s	21.2s	20.3s
5th	y-axis	15.5s	15.1s	17.0s
41st	y-axis	7.2s	7.4s	7.6s
44th	z-axis (vertical)	7.0s	7.0s	6.9s
46th	rx-axis (torsional)	6.7s	6.8s	6.7s
47th	rx-axis	6.6s	6.4s	6.4s
48th	rx-axis	6.6s	6.3s	6.3s

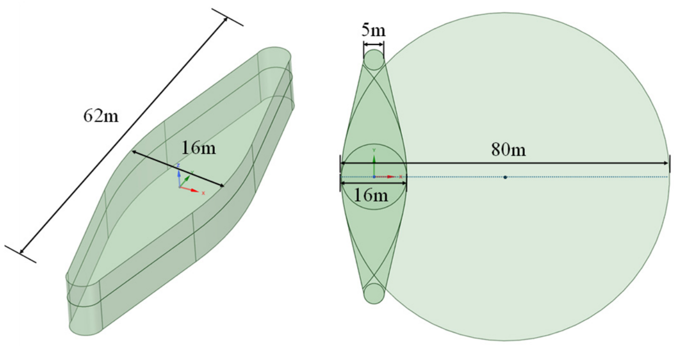

Figure 2. Dimensional specifications of the pontoon

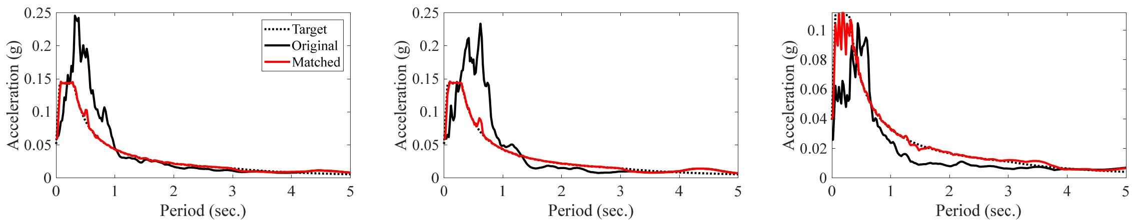

(a) x-acceleration (b) y-acceleration (c) z-acceleration

Figure 3. Maximum response acceleration as function of system's natural periods: Target vs Original vs Matched

We selected an earthquake record of moment magnitude (MM) 6.8 that occurred in California and up-scaled it by the spectral matching method [18]. The target spectrum is based on South Korea with soil class of soft ground, and the vertical design spectrum is assumed 77% of the horizontal spectrum, as shown in Figs. 3(a)-3(c). In Fig. 3, the matched one agrees well with the given target values. Two horizontal (x and y) and a vertical (z) ground motion (acceleration) time-series for original and matched cases are given in Figs. 4(a), and the corresponding power spectral densities

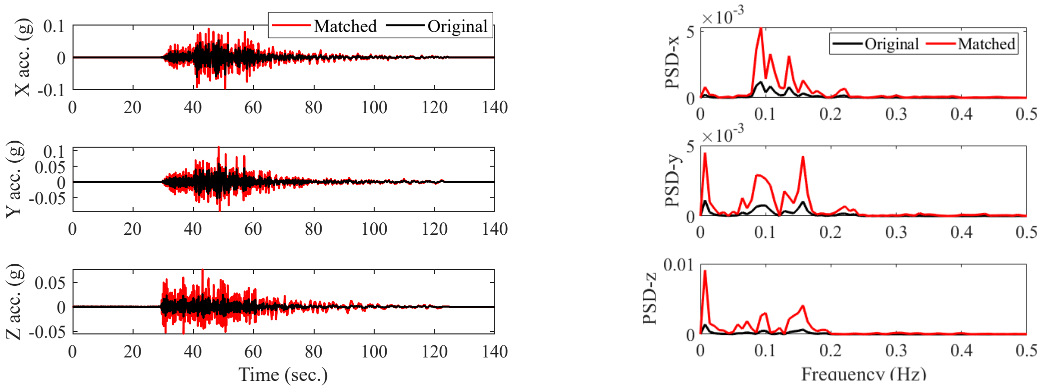

(a) Ground acceleration time-series

(b) Ground displacement PSD (Unit: cm^2/Hz)

Figure 4. Ground motion: Original vs Matched

Table 3. Load case table I: intact; F: pre-failure; T: sudden-failure (transient)

Case #	Condition	Failure
1		I
2	Earthquake (S5, 200 YRP)	F
3		T

(PSDs) of ground displacement are in Figs. 4(b). The matched seabed-earthquake time series and spectra are shown to be larger compared to the California earthquake condition due to different soil conditions. The failed line was selected based on the estimated maximum mooring line tension under the present ground motion, as studied in [11], which means that it is most likely to fail first. It should be noted that the submarine-earthquake-induced hydroacoustic wave loads, the so-called seaquake load, is neglected in this study; one may refer to [14, 19].

3.2 Numerical results and analyses/discussions

Fig. 5 presents pre-tensions for the intact and one-line pre-failure cases at the selected mooring lines. The four selected lines are #2, 10, 18, and 26, and the failed line is #12 as marked in green in Figs. 1(a) and 1(b). As a result of the pre-failure, the pre-tension at the neighboring line #10 is the most increased by 192 kN compared to that of the intact case since the neighboring lines share the most burden of the line failure.

Fig. 6 compares the selected pontoon's 3-DOF (degrees-of-freedom) translational-displacement time series among the three different I-F-T scenarios. As shown in Fig. 1(b), the failed line is connected to pontoon #14. Accordingly, it is observed that the transverse mean offset of pontoon #14 is the largest, about 0.78 m along the *y*-axis. In the cases of I and F, the dynamic responses of the pontoons are not much different from each other. However, the sudden-failure scenarios clearly reveal significant transient responses with noticeable overshoots, especially along the y- and z-axes. Since the failed line is connected to pontoon #14, it is obvious that the largest discrepancies between F and T are observed from this pontoon. Pontoon #18 also has significant transverse (y) displacements due to being close to the failed line #12 without mooring restriction.

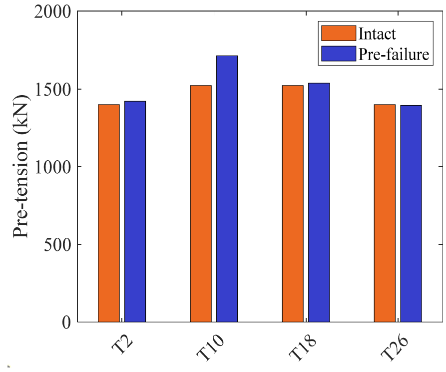

Figure 5. Pre-tensions at selected mooring lines

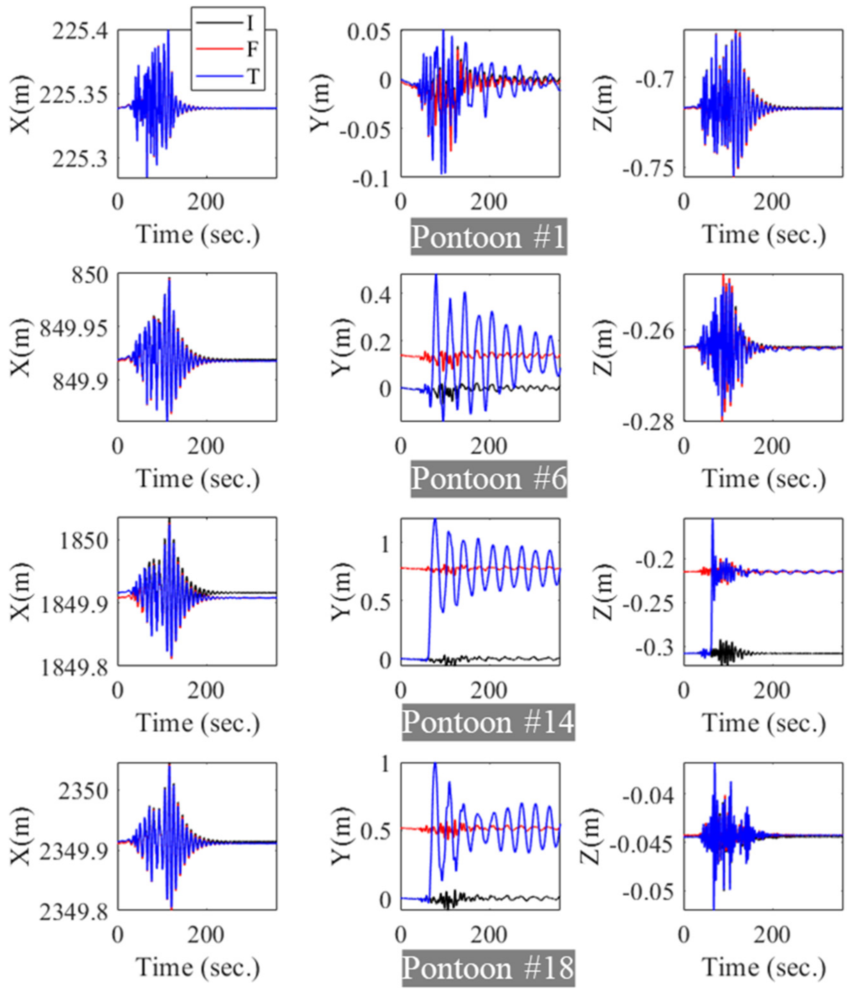

Figure 6. Pontoon 3-DOF translational motion time-series: from top to bottom #1, 6, 14, 18 pontoons

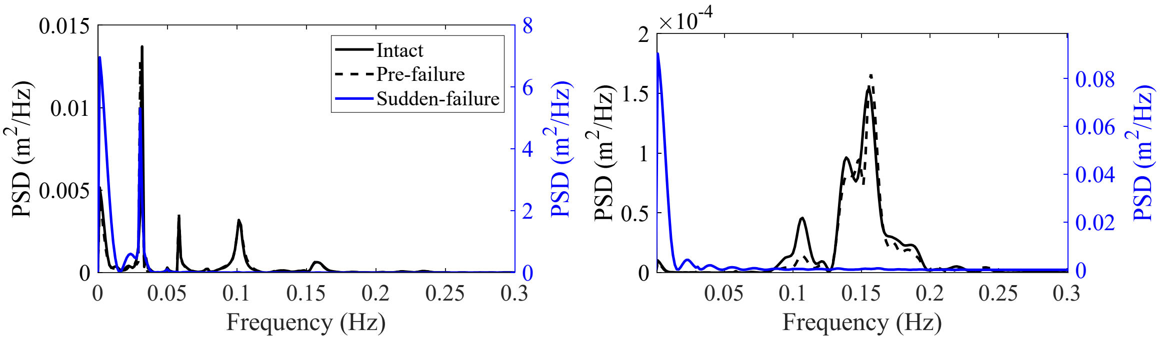

Figure 7. Power spectral densities (PSDs) of pontoon #14 displacements

We further checked the power spectral densities (PSDs) of the y- and z-displacements of pontoon #14 in Figs. 7(a) and 7(b). The response due to the sudden-failure has different scales compared to the other two I-F cases, and it also shows a larger low-frequency (nearly zero-frequency) peak due to the shifting of the equilibrium (offset) position and the low-frequency component of seismic excitation (about 0.0007 Hz) as shown in Fig. 4(b). Further, the oscillation observed in the y-displacement after the initial overshoot is connected to another peak frequency of 0.03 Hz in Fig. 7(a) which is a free-vibration response at the natural frequency. Indeed, this is consistent with the natural period of the lowest transverse bending mode (about 32-34 seconds) as shown in Table 2. Meanwhile, such noticeable oscillation is not observed for the z-displacement in both the time-series and PSD of the sudden-failure scenario. On the other hand, a large response is observed around 0.15 Hz in the intact and pre-failure cases, which is consistent with the natural period of the vertical bending mode (approx. 0.14 Hz) and the peak frequencies of the ground motions in Fig. 4(b). The other multiple peaks, especially at 0.1 Hz, in Figs. 7(a) and 7(b) in the intact and pre-failure scenarios are associated with the frequency content of the imposed seabed motions. It is observed from Fig. 7(b) that a slight discrepancy occurs at 0.1 Hz in the *Z*-PSD between the intact and pre-failure cases, but interestingly the intact case has a slightly higher response. This is due to the fact that the seabed motion is transferred through the mooring lines, thereby the portion of the failed line cannot contribute to the seismic excitation of the pontoon. On the other hand, since the failed line decreases the pontoon's station-keeping performance, other types of excitations, e.g., waves, currents, and wind, would definitely increase the pontoon's motion amplitudes in the failed condition although the typical frequencies of such environmental excitations are site-specific.

We further analyzed the statistics of the y-displacement along the girders in Fig. 8(a) and the corresponding statistics of the horizontal bending moment with respect to z-axis in Fig. 8(b). It should be noted that the left end of the bridge is clamped, i.e., both the translational and angular displacements are fixed, while the right end is pinned with respect to y and z axes. Thereby, the bending moment is maximized on the left end whereas it goes to null at the opposite position. Accordingly, the y-displacement tends to smoothly vanish as it approaches the left end whereas it rapidly decays to zero in the vicinity of the right end. Consequently, the dynamic responses are significantly affected by the types of constraints. Indeed, a sensitivity study for different types of end-constraints has been conducted by the present authors [3], and it is evident that sophisticated modeling of the end conditions is essential to better estimate realistic static and dynamic responses.

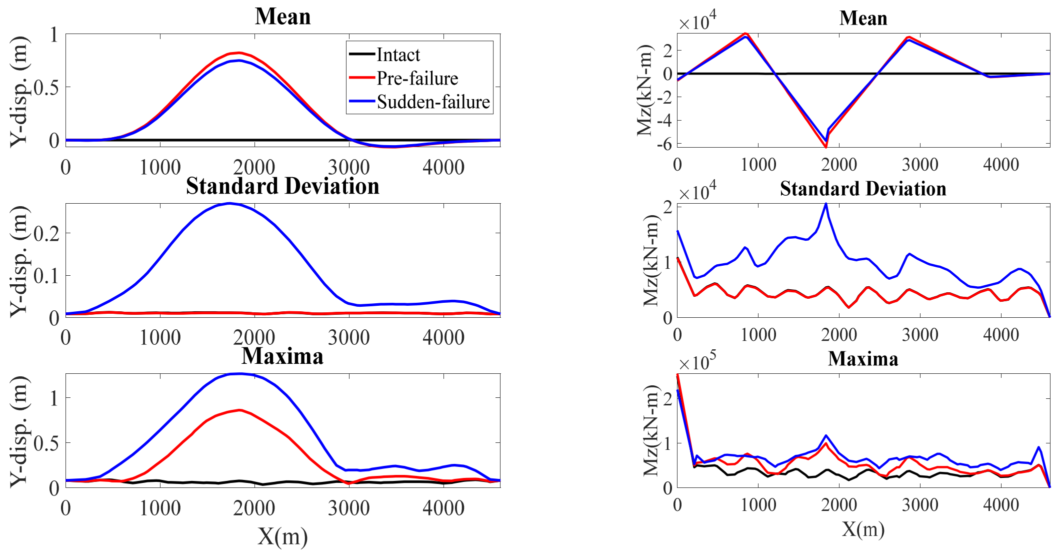

(a) Girder Y-displacement statistics across the bridge

(b) Girder horizontal bending moment statistics across the bridge

Figure 8. Statistics of girder y-displacement and horizontal bending moment Mz

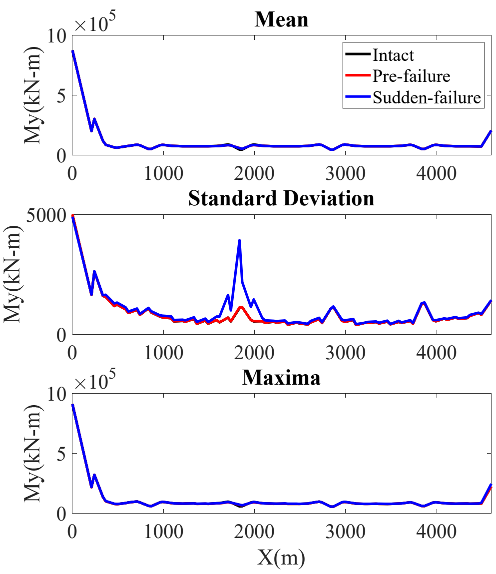

Figure 9. Statistics of girder vertical bending moment My between I (intact; black), F (pre-failed; red) and T (sudden-failure during earthquake; blue)

In general, the transient effects due to the sudden disconnection of one line dominate over the other two scenarios in both the girder transverse displacement and transverse bending moment especially in the standard deviation. However, the transient effects become less important at the clamped left end, where maximal Mz occurs. It is interesting to see that Case F shows a higher

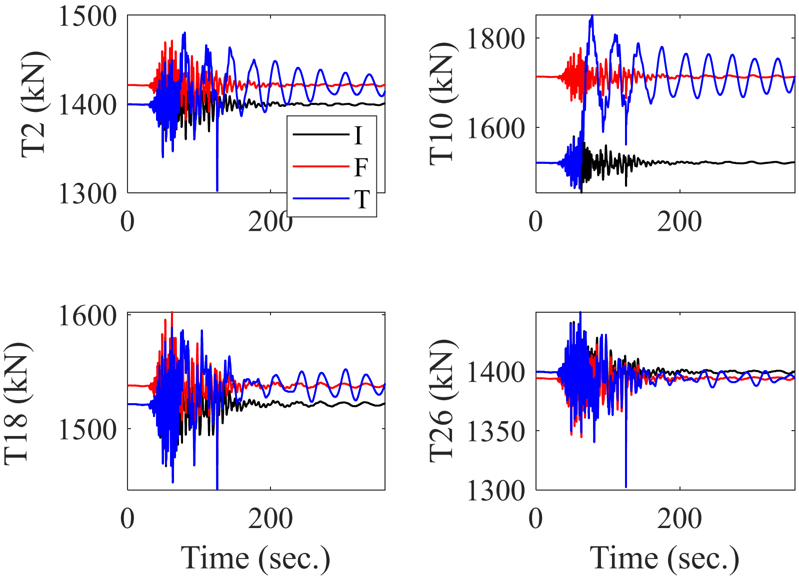

Figure 10. Mooring fairlead tensions: Lines #2, 10, 18, 26 (I: intact; F: pre-failed; T: sudden-failed)

bending moment at the left clamped end than Case T even though the standard deviation is higher in the sudden-failure scenario. It may depend on the phase differences between the earthquake-induced and transient responses i.e. partial cancellation by the two components.

In Fig. 9, the same statistics are shown for vertical bending moment My along the entire girder length. In this case, we observe a significant increase in standard deviation due to transient effects only near the failed mooring line, which can be expected from the corresponding vertical displacements of pontoons shown in Fig. 6. Since the dynamic effects are rather small compared to dominant static values in the vertical bending moment My, the mean and maximum values are almost identical along the entire girder.

In Fig. 10, the fairlead tension time-series of the selected mooring lines (#2, #10, #18, and #26) are presented for the three scenarios. It is seen that one of the mooring lines (#10) within the cluster of the failed line (i.e., the lines fastened to the pontoon #14) experiences the largest increase in tension magnitude. In case of the pre-failed condition, the dominant effect is the increase of mean tension caused by the increase of burden corresponding to the changed mean horizontal offset of the pontoon after failure as previously observed in Fig. 5. In case of the sudden-failure condition, in addition to the same mean-tension shift, there is also a significant increase of dynamic tension due to the transient overshooting followed by subsequent transient motions of the pontoon. The transient-motion-induced dynamic tensions decay in amplitude with time but persist even after the seabed earthquake is subsided. The transient effect is very important for the mooring lines within the same cluster of the failed line. We also observe that the transient motions occur at the system's lowest transverse natural frequency as can be predicted by physics. For other mooring lines, these kinds of transient effects are also observed but they play much less role in view of maximum mooring tension.

Further, we checked the PSD of the line #10 tension in Fig. 11. The sudden-failure case shows large peak in the lowest-frequency region due to the sudden shift of horizontal offset. The

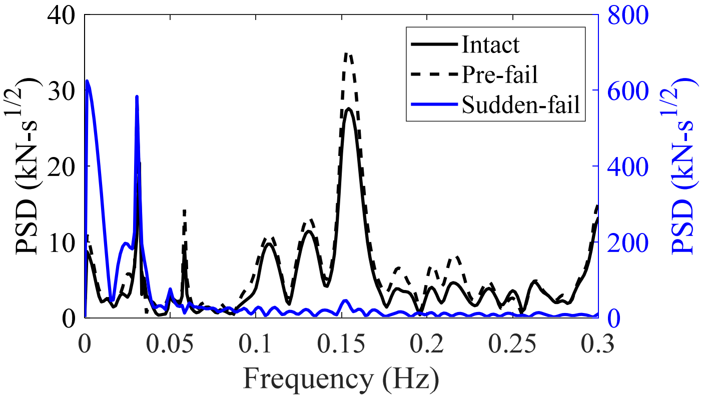

Figure 11. Square-root of PSD of fairlead tension in mooring line #10

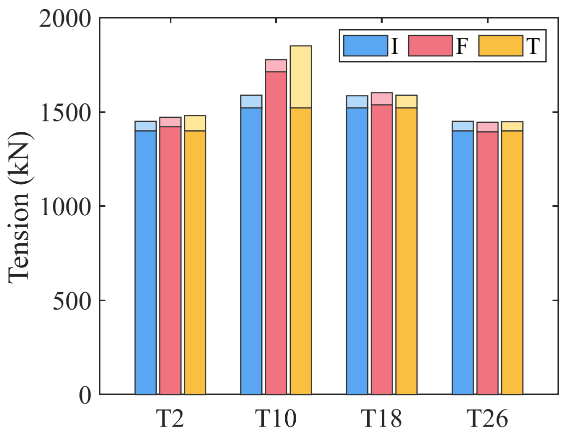

Figure 12. Maximum tensions of mooring lines #2, 10, 18, 26: lower (brighter) part is pre-tension; upper (darker) part is maximum dynamic tension. (I: intact; F: pre-failed; T: sudden-failed)

neighboring peak corresponds to the transient motions at the lowest transverse bending mode and its natural frequency as given in Table 2. Those two transient effects are dominant over earthquake-induced dynamic tensions. On the other hand, the pre-failure and intact cases are also plotted in Fig. 11. The pre-failure case is higher at 0.15 Hz but lower around 0.4 Hz than that of the intact case. The former peak corresponds to the lowest vertical bending mode and is also observable in the pontoon's z-displacement PSD in Fig. 7(b). The second frequency is expected to be the natural period of the mooring lines, as it is found neither in the PSD of the ground motion nor among the natural periods of the floating bridge. However, if one looks at the scales of three scenarios (order of magnitudes), the sudden-failure case is dominant over the other two cases.

The maximum static and dynamic tensions for the selected four mooring lines are presented in Fig. 12. The brighter part stands for the dynamic tension and the darker part stands for the pre-tensions. It shows that most portions of the maximum mooring tensions are caused by the initial tensions (pre-tensions). The tension of line #10 within the same cluster of the failed line shows the largest dynamic tension in the sudden-failure case, which corresponds to 21.6% of the pre-tension.

4. Conclusions

In this study, we carried out a numerical study to investigate the transient response of a floating bridge due to the sudden-failure of a mooring line under seabed earthquakes, for which bridge-mooring coupled time-domain dynamic simulation program was utilized. The dynamic responses of the selected pontoons, statistical values of displacements and bending moments along the girders, and fairlead tensions of the selected mooring lines were compared among three different scenarios: (i) intact; (ii) 1-line pre-failure; (iii) 1-line sudden-failure. From the simulation results, the following concluding remarks were drawn:

- In the sudden-failure case, the transient responses of the pontoons and the corresponding effects on neighboring-mooring tensions can be important, which are absent in the intact and pre-failure cases. The transient transverse motions occur at the natural frequency of the lowest transverse bending mode right after the failure. The magnitudes of the transient tensions are large and comparable to the increase of mean tension after line failure in neighboring lines.
- The pre-failure case does not produce such transient effects and only accounts for earthquake-induced dynamic responses. In the pre-failure case, however, the increase of mean tension on other lines without the failed line can be accounted for.
- The transverse structural responses and transverse bending moments of girders are also appreciably influenced by the transient effects after sudden line failure. In case of the vertical bending moment of girder, the transient effects become less important since its static components by the weight distribution are dominant.
- The increases in the fairlead tensions of the adjacent mooring lines due to the sudden failure of a line are noticeable (e.g. 21.6% of the pre-tension in the present case). Nevertheless, the major portion of the maximum tension is given by the mean-tension increases and the pre-tensions.

Without loss of generality, the present study can be extended to the combined wind/wave/current sea condition and the propagating seismic wave over distances to cause phase-lag effects.

References

1. Jang, M., Lee, Y., Kim, S., Kang, Y.J. (2020). Dynamic behavior of a long-span cable-stayed bridge with floating towers after the sudden failure of tethers and cables under irregular waves. Journal of Marine Science and Technology, 28(6), 14. https://doi.org/10.6119/JMST.202012_28(6).0014.
2. Dai, J., Leira, B.J., Moan, T., Kvittem, M.I. (2020). Inhomogeneous wave load effects on a long, straight and side-anchored floating pontoon bridge. Marine Structures, 72, 102763. https://doi.org/10.1016/j.marstruc.2020.102763.
3. Lee, I., Kim, M., Song, J., Kim, S. (2024). Dynamic analysis of floating bridges under combined earthquakes and waves. Ocean Systems Engineering, 14(2), 115-139. https://doi.org/10.12989/ose.2024.14.2.115.
4. MultiConsult. (2017). Bjørnafjorden, straight floating bridge phase 3. Analysis and design (Base Case).
5. Jin, C., Kim, M., Chung, W.C., Kwon, D.S. (2020). Time-domain coupled analysis of curved floating bridge under wind and wave excitations. Ocean Systems Engineering, 10(4), 399-414. https://doi.org/10.12989/ose.2020.10.4.399.
6. Kwon, J.S. (2005). Seismic response analysis of a floating bridge with discrete pontoons. Journal of the Earthquake Engineering Society of Korea, 9(2), 47-58.

7. Song, J., Shin, H., Jin, C., Kim, S. (2025). Simplified analysis method for pontoon-supported floating bridges under waves. Ocean Engineering, 324, 120758. https://doi.org/10.1016/j.oceaneng.2025.120758.
8. Yan, J., Liu, J., Liu, Z., Guo, A. (2024). Experimental study on the effects of hydrodynamic loads on the seismic response of end-anchored floating bridges. Ocean Engineering, 300, 117464. https://doi.org/10.1016/j.oceaneng.2024.117464.
9. Yan, J., Liu, J., Liu, Z., Li, H., Guo, A. (2023). Experimental study on the dynamic responses of the end-anchored floating bridge subjected to joint actions of earthquakes and water waves. Earthquake Engineering and Structural Dynamics, 52(10), 2945-2965. https://doi.org/10.1002/eqe.3904.
10. Jin, C., Kim, S., Chung, W.C., Kang, B., Kim, S. (2024). Feasibility investigation of tuned mass damper for vibration control of curved floating bridge in winds and waves. Applied Ocean Research, 148, 104013. https://doi.org/10.1016/j.apor.2024.104013.
11. Lee, I., Kim, M., Song, J., Kim, S. (2025). The effect of a mooring line failure on the dynamic response of a floating bridge under seismic excitation. ISOPE International Ocean and Polar Engineering Conference.
12. Park, J.Y., Lee, I.J., Kim, M.H., Jin, C., Mishra, I., Griffith, D.T., Rotea, M. (2026). Automatic mooring-line-failure detection by using hull motion sensor and ML (Machine Learning) for FOWT (Floating Offshore Wind Turbine), Applied Ocean Research, 165, 104844. https://doi.org/10.1016/j.apor.2025.104844.
13. Jebari, O.1, Kwon, D.S., Kim, S.J., Jin, C., Kim, M.H. (2025). Machine learning-based mooring failure detection for FPSOs: a two-step ANN approach. Journal of Marine Science and Engineering, 13(4), 791. https://doi.org/10.3390/jmse13040791.
14. Lee, I., Kim, M. (2026). Seaquake loads by a hybrid integral-equation method for dynamic analyses of floating offshore wind turbines under seabed earthquakes. Marine Structures, 109, 104093. https://doi.org/10.1016/j.marstruc.2026.104093.
15. Lee, C.H. (1995). WAMIT theory manual. Massachusetts Institute of Technology, Department of Ocean Engineering.
16. Orcina. (2024). OrcaFlex manual. Orcina Ltd.
17. Cummins, W. (1962). The impulse response function and ship motions.
18. Al Atik, L., Abrahamson, N. (2010). An improved method for nonstationary spectral matching. Earthquake Spectra, 26(3), 601-617. https://doi.org/10.1193/1.34591.
19. Lee, J.H., Kim, J. K. (2015). Dynamic response analysis of a floating offshore structure subjected to the hydrodynamic pressures induced from seaquakes. Ocean Engineering, 101, 25-39. https://doi.org/10.1016/j.oceaneng.2015.04.010.